Ensemble-Based Assimilation of Satellite All-Sky Microwave Radiances Improves Intensity and Rainfall Predictions for Hurricane Harvey (2017)

Yunji Zhang[1], Scott B. Sieron[2], Yinghui Lu[3], Xingchao Chen[1], Robert G. Nystrom[4], Masashi Minamide[5], Man-Yau Chan[1], Christopher M. Hartman[1], Zhu Yao[1], James H. Ruppert, Jr.[6], Atsushi Okazaki[7], Steven J. Greybush[1], Eugene E. Clothiaux[1], and Fuqing Zhang[1†]

[1]Department of Meteorology and Atmospheric Science, and Center for Advanced Data Assimilation and Predictability Techniques, The Pennsylvania State University, University Park, Pennsylvania

[2]I.M. Systems Group Inc. (IMSG) at NOAA/NWS/NCEP/EMC

[3]Nanjing University, Nanjing China

[4]National Center for Atmospheric Research (NCAR)

[5]Department of Civil Engineering, The University of Tokyo, Tokyo, Japan

[6]School of Meteorology, The University of Oklahoma, Norman, OK

[7]Department of Global Environment and Disaster Prevention Sciences, Hirosaki University, Hirosaki, Japan

Corresponding author: Yunji Zhang (yuz31@psu.edu)

†Deceased.

Key Points:

- Satellite all-sky infrared and microwave radiances are assimilated to assess their impacts on forecasts for Hurricane Harvey.
- Along with infrared radiances, microwave radiances improve the track and intensity forecasts for Harvey.
- Microwave radiance assimilation leads to better analyses of the hydrometeor fields and more accurate rainfall forecasts.

Abstract

Ensemble-based data assimilation of radar observations across inner-core regions of tropical cyclones (TCs) in tandem with satellite all-sky infrared radiances across the TC domain improves TC track and intensity forecasts. This study further investigates potential enhancements in TC track, intensity, and rainfall forecasts via assimilation of all-sky microwave radiances using Hurricane Harvey (2017) as an example. Assimilating GPM constellation all-sky microwave radiances in addition to GOES-16 all-sky infrared radiances reduces the forecast errors in the TC track, rapid intensification, and peak intensity compared to assimilating all-sky infrared radiances alone, including a 24-hour increase in forecast lead-time for rapid intensification. Assimilating all-sky microwave radiances also improves Harvey's hydrometeor fields, which leads to improved forecasts of rainfall after Harvey's landfall. This study indicates that avenues exist for producing more accurate forecasts for TCs using available yet underutilized data, leading to better warnings of and preparedness for TC-associated hazards in the future.

Plain Language Summary

Track, intensity, and rainfall are fundamental elements of all forecasts and warnings associated with tropical cyclones (TCs). Over the last few decades, the forecast community has significantly improved TC track forecasts. Notable improvements in TC intensity forecasts have recently been achieved using high-resolution models and remote-sensing observations over the inner-core region of TCs. This study builds on these earlier efforts by investigating the impacts of utilizing microwave observations on the forecast accuracy of TC track, intensity, and rainfall. Because microwave radiances are sensitive to water vapor, liquid water, and ice, using these observations in TC computer forecasts is expected to improve estimates of the liquid water and ice within TCs, which can then lead to better rainfall forecasts. These expectations are borne out in our study's tests with Hurricane Harvey. These results indicate that incorporating currently available yet underutilized observations into TC computer forecasts can further improve warnings of, and preparedness for, TC-associated hazards in the future.

1 Introduction

Tropical cyclones (TCs; see Appendix A for a complete list of acronyms) are among the most devastating natural disasters in the tropics and mid-latitudes. They make for a triple-threat of wind damage, surge inundation, and inland/freshwater flooding, the last of which is a leading cause of fatalities in the United States from TCs (Rappaport 2014). Accurate predictions of TCs are valuable to society because these predictions facilitate targeted and efficient preparations for mitigating the loss of life and property.

While forecasts of TC track and intensity have been continually improving over recent decades (e.g., DeMaria et al. 2014, Cangialosi et al. 2020), one important remaining challenge is the accurate prediction of hazardous TC precipitation (Kidder et al. 2005). Hazardous TC precipitation events are difficult to predict because such events often result from the hard-to-predict TC rain bands [e.g., Hurricane Harvey (2017); Blake and Zelinsky, 2018] and long-distance interactions (Galarneau et al. 2010, Meng and Zhang 2012). The forecast challenges associated with the inner (e.g., Montgomery and Kallenbach 1997, Wang 2002) and outer (e.g., Diercks and Anthes 1976, Chow et al. 2002) spiral rain bands are multi-faceted: spiral rain bands' existence, intensity, storm-relative location, and small-scale structures are difficult to

forecast accurately. Consequently, rainfall forecasts, such as from the Weather Prediction Center (WPC), often cover a broad area and come with an expected range of rain accumulations tagged with footnotes of possible localized extreme values.

Some of the most important observations of TCs over the ocean are satellite infrared (IR) and microwave (MW) brightness temperatures (BTs; used interchangeably with radiance hereafter). IR sensors onboard geostationary satellites provide seamless, high-spatiotemporal-resolution BTs of the tropics and the subtropics. They are sensitive to the absorption and emission of IR radiation associated with water vapor and hydrometeors, hence provide information on cloud locations, cloud-top heights, and atmospheric moisture in cloud-free regions. IR BTs are also one of the critical components of the Dvorak technique for estimating TC intensity (Dvorak 1975; Velden et al. 2006). While MW BTs are much less sensitive to cloud particles, they are sensitive to the absorption and scattering of MW radiation associated with larger precipitation-related hydrometeors. Therefore, passive MW BTs are often used in assessing TC structure and intensity and contributing to operational products from the National Hurricane Center (NHC) that include information on low- and mid-level circulations of pre-TC disturbances that would otherwise be obscured by the outflow anvil clouds of deep convection, and secondary eyewalls and potential eyewall replacement cycles for mature TCs.

While IR and MW BTs are heavily used in the qualitative assessment of TCs, they are still underutilized in operational global and regional models for TC prediction (Geer et al. 2018, Gustafsson et al. 2018). Recently, studies examining the ensemble-based assimilation of all-sky (i.e., both clear-sky and cloud-affected) IR BTs into regional models have demonstrated its potential in improving TC forecasts (Minamide and Zhang 2018, Honda et al. 2018, Zhang et al. 2019, Hartman et al. 2021). However, IR BTs contain little direct information on precipitation that may exist below opaque cloud tops. For these conditions, techniques like the ensemble Kalman filter (EnKF) rely on ensemble covariances to update the model state underneath the cloud tops. Unfortunately, these covariances are sometimes erroneous because of the limited ensemble size (Zhang et al. 2021a, b).

On the other hand, MW BTs are able to reflect the distributions of hydrometeors underneath the cloud tops, providing information in regions that are unobservable for the IR BTs. Recent demonstrations of realistic correlations between all-sky MW BTs and TC intensity and structure (Zhang et al. 2021c) motivate studying the potential benefits of simultaneously assimilating all-sky MW BTs and all-sky IR BTs for the analysis and prediction of TCs. In this work, we employ Hurricane Harvey (2017) as a case study. This study expands upon recent efforts in employing ensemble-based assimilation of all-sky MW BTs for TCs (e.g., Wu et al. 2019; Sieron 2020; Kim et al. 2020; Christophersen et al. 2021; Xu et al. 2021) by examining the impacts of all-sky MW BTs on TC's track, intensity, and rainfall forecasts.

2 Methodology

For this study, we utilized the PSU WRF-EnKF data assimilation and forecast system (Zhang and Weng 2015; Weng and Zhang 2012, 2016; Zhang et al. 2009, 2011, 2016; Chen and Zhang 2019; Chan et al. 2020). The system configuration largely follows previous studies by Zhang et al. (2019) and Minamide et al. (2020), except that we adopted the Thompson (2008) microphysics scheme. Following Sieron et al. (2017, 2018), non-spherical ice-hydrometeor

scattering properties consistent with the microphysics are included to realistically simulate the MW BTs. AOEI (Minamide and Zhang 2017; for both IR and MW BTs) and ABEI (Minamide and Zhang 2019; for IR BTs only) are applied to mitigate the deleterious impacts of strong nonlinearities in the assimilation of all-sky BTs.

Because multiple studies have demonstrated that all-sky IR BT assimilation improves forecasts of TC track and intensity (e.g., Zhang et al. 2016, 2019; Honda et al. 2018; Minamide and Zhang 2018; Minamide et al. 2020; Hartman et al. 2021), the baseline experiment for this study assimilates conventional surface and upper-air observations from the GTS, TC center pressure information from TCVitals, and hourly all-sky IR BTs from channel 8 (6.2-μm) of the GOES-16 ABI. This experiment is called "IR-only" hereafter. BTs from ABI's channel 8 are mostly sensitive to moisture in the upper-troposphere in clear-sky regions, and our group has had success assimilating them in many previous TC studies (Minamide and Zhang 2017, 2018, 2019; Zhang et al. 2019; Minamide et al. 2020; Hartman et al. 2021).

The benefits of assimilating all-sky MW BTs are evaluated through an experiment that assimilates all-sky MW BTs from the GPM constellation sensors (Hou et al. 2014; Skofronick-Jackson et al. 2017; see Appendix B for a complete list of assimilated channels) in addition to all observations assimilated in the IR-only experiment. This second experiment is called "IR+MW" hereafter. We used GPM constellation sensors' BTs in this study because they underwent extensive quality control and cross-calibration. MW BTs from two channels are assimilated: the ~19 GHz vertically polarized low-frequency channel ("the LF channel" hereafter; only assimilated over the ocean because of uncertainties in modeled land emissivity) and the 183.31±6.6 GHz high-frequency channel ("the HF channel" hereafter; assimilated everywhere because surface contributions at this frequency are negligible for our purposes). These two channels were selected for a litany of reasons (Sieron 2020): they are sensitive to liquid (the LF channel) and ice (the HF channel) water contents, have the best one-to-one correspondence between water content and changes against clear-sky BTs, have less sensitivity to non-water-content atmospheric/surface properties, have high climatological agreements between observed and simulated BTs for precipitating regions in the EnKF priors, and have the highest frequency of occurrence across all sensors in the observing system. Of the channels in the 183-GHz family, the ±6.6-GHz channel is chosen because its clear-sky weighting function peaks in the lower troposphere, making it complementary with the ABI channel 8 IR BT whose weighting function peaks at higher altitudes (Zhang et al. 2021c). Channels around 89 GHz are used for those sensors that do not have a channel near 183 GHz.

We initialize both IR-only and IR+MW experiments at 0000 UTC 22 August with 60 ensemble members that contain random perturbations generated by WRFDA and performe cycling EnKF data assimilation from 1200 UTC 22 August to 0000 UTC 25 August. Deterministic forecasts out to 0000 UTC 27 August are produced from the EnKF analysis mean every 6 hours, starting from 1800 UTC 22 August. 23 out of the 61 EnKF cycles assimilates all-sky MW radiances, 17 of which include MW BTs from both LF and HF channels and the remaining 6 cycles include only HF channel BTs.

3 Results

We first examine how the analysis-to-observation fits change from the IR-only experiment to the IR+MW experiment. We then compare the forecast performances of the two

experiments in terms of their forecasts of TC Harvey's track, intensity, and rainfall amount after landfall.

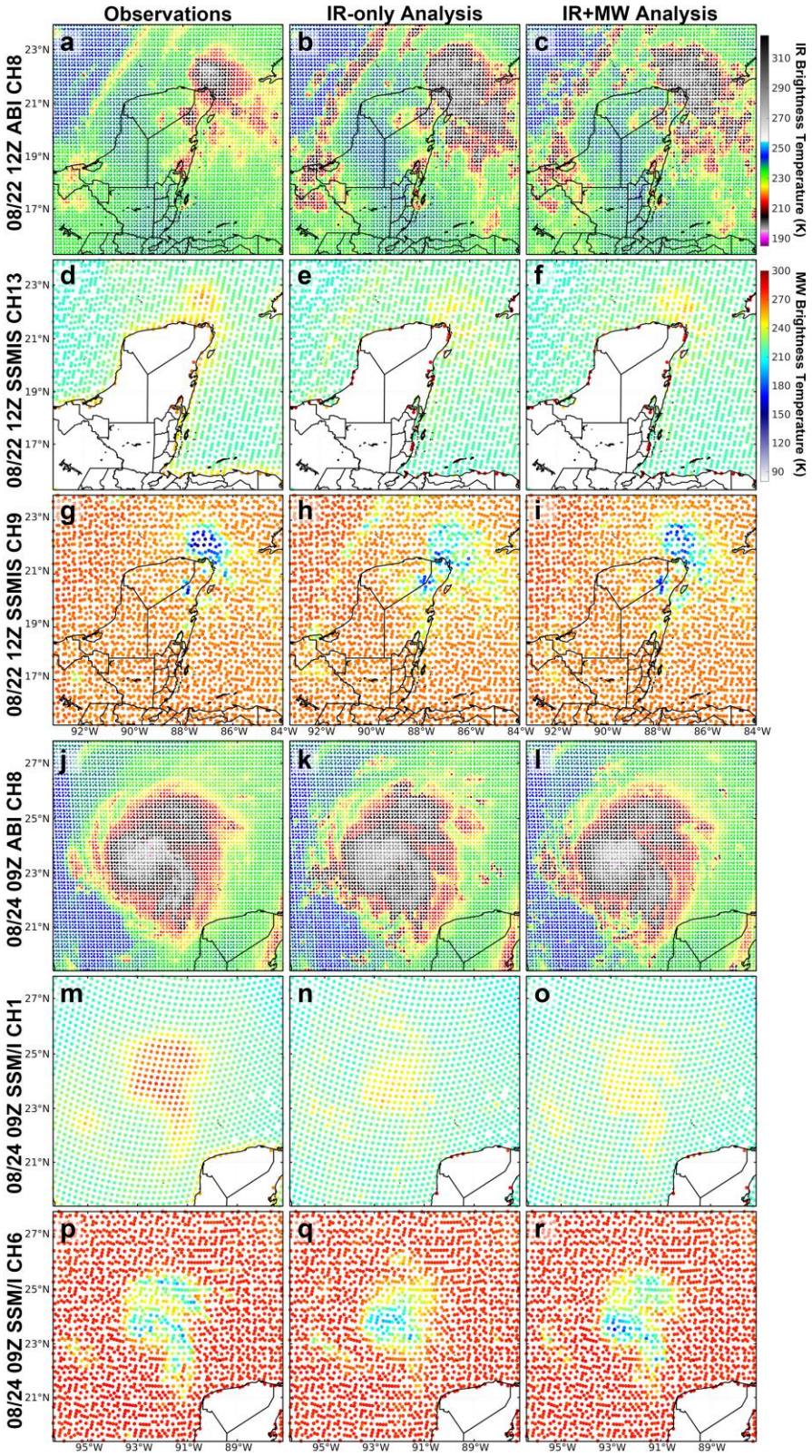

Figure 1. (first column) Observed and (second and third columns) simulated BTs from the EnKF analysis ensemble mean at (a)–(i) 1200 UTC 22 August and (j)–(r) 0900 UTC 24 August for (a–c, j–l) ABI channel 8, (d–f, m–o) the MW LF channel, and (g–i, p–r) the MW HF channel.

3.1 Comparison of EnKF analyses

We first compare simulated IR and MW BTs from the analyses from the first EnKF cycle (1200 UTC 22 August) against the assimilated observations (Figs. 1a-i), which qualitatively reveal the changes with the assimilation of these observations. Both IR-only and IR+MW experiments show simulated IR BTs that are qualitatively similar to the observations (Figs. 1a–c). More importantly, while both experiments overestimate the coverage of the cold cloud tops within the domain, the overestimation is milder for the IR+MW experiment (Fig. 1c). Furthermore, near the tip of the Yucatan Peninsula, the IR+MW analysis better captured the warm LF MW BTs (Figs. 1d,f) and the cold HF MW BTs values (Figs. 1g,i) than the IR-only analysis (Figs 1e, h). These differences in MW BTs suggest that the IR+MW analysis better captured the abundant liquid and ice hydrometeors in that region. Since both experiments have identical priors at this first cycle, the differences in their analyses at this time are solely associated with the assimilation of the MW BTs. The first cycle's results thus indicate that the inclusion of MW observations can improve the analyzed hydrometeor fields. It is also worth noting that the match between the IR+MW analysis and the observations is noticeably better than found in the previous studies of Wu et al. (2019). We attribute this improvement to the microphysics-consistent non-spherical ice-particle scattering tables developed for CRTM by Sieron et al. (2017, 2018) and the use of AOEI (Minamide and Zhang 2017).

We also compared the two experiments' analyses against the IR and MW observations shortly after the onset of Harvey's rapid intensification (RI). Figures 1j–r show the observed and simulated BTs at 0900 UTC 24 August, which is the first EnKF cycle with available MW BTs after the onset of Harvey's RI, and 8 hours after the most recent cycle that included MW BT assimilation. At this point, clouds and rainband structures that are typical of TCs are apparent in both the IR and MW observations (Figs. 1j,m,p). The cumulative effects of the cycling EnKF resulted in close matches between both experiments' simulated IR BTs (Figs. 1k,l) and the observations (Fig. 1j). However, both experiments' analyses noticeably underestimated the amount and areal extent of the liquid hydrometeors, indicated by the cooler-than-observed warm LF MW BTs. Systematic cold biases in both experiments for the LF MW channel is beyond the scope of this study but needs further investigation, and may be related to biases in the microphysics scheme, as the Thompson et al. (2008) microphysics scheme is known to underpredict rainwater (e.g., Conrick and Mass 2019).

The inclusion of the MW observations also improved the analysis in terms of the HF MW channel. According to Figure 1q, the IR-only analysis exhibits a cold center that matches reasonably with the observations but fails to capture the secondary cold centers to the northeast and southeast of the TC center. These missing two features are associated with intense outer rainbands (Fig. 1q). With the assimilation of all-sky MW radiances, these missing rainbands are better captured (Fig. 1r). The primary rainband that extends southward from the TC center is particularly well-represented in IR+MW. This implies that the addition of MW observations to data assimilation improves the analyzed rainbands.

In summary, the addition of MW observations resulted in analysis improvements for both the IR and MW observations. These BT improvements indicate improvements to the analyzed

structure and distribution of hydrometeors of Harvey. Next, we examine how these improvements impact Harvey's track, intensity, and rainfall forecasts.

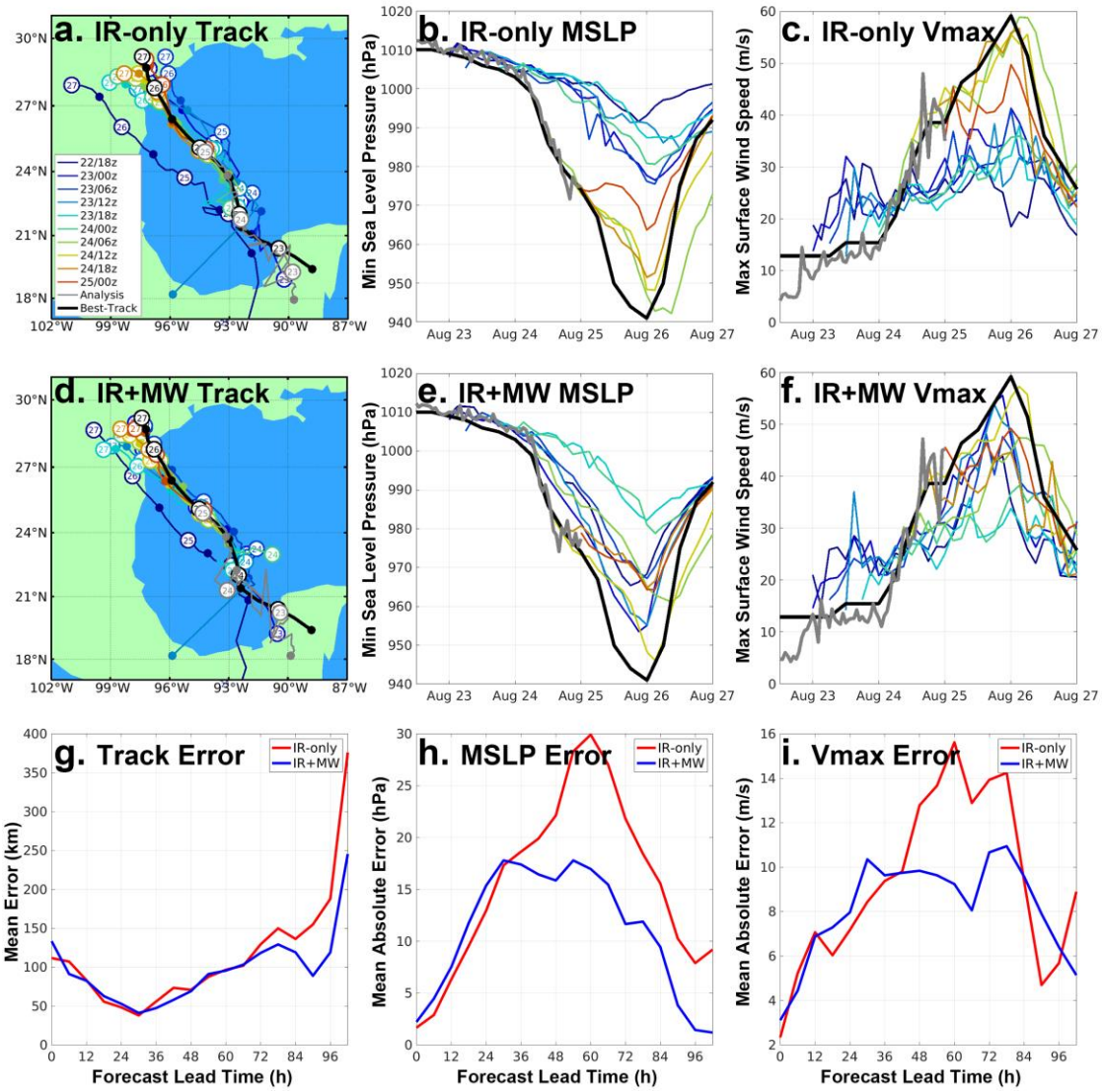

Figure 2. Analyses and forecasts of (first column) track, (second column) minimum sea-level pressure, and (third column) maximum surface wind speed for the (first row) IR-only and (second row) IR+MW experiments. (third row) Errors in the forecasts verified against NHC's best-track analysis.

3.2 Comparison of deterministic forecasts

Figure 2 shows the analyses and forecasts of Hurricane Harvey's track and intensity for the IR-only and IR+MW experiments, as well as associated forecast errors with respect to the forecast lead time. Both the IR-only and IR+MW experiments predict the track with reasonable accuracy, especially for forecasts that are initialized relatively late. Additionally, the westward biases in the 1800 UTC August 22 forecast and the eastward biases in the three forecasts from 0000 UTC to 1200 UTC August 23 of the IR-only experiment (Fig. 2a) are noticeably reduced in

the IR+MW forecasts (Fig. 2d). Although reduced errors in these forecasts are diluted after averaging across all 10 forecasts, the track forecast errors in the IR+MW experiment are slightly smaller, overall, than in the IR-only forecasts beyond 72 h (Fig. 2g), although it is not statistically significant at 95% confidence level using a Wilcoxon signed-rank test (Wilks 2011).

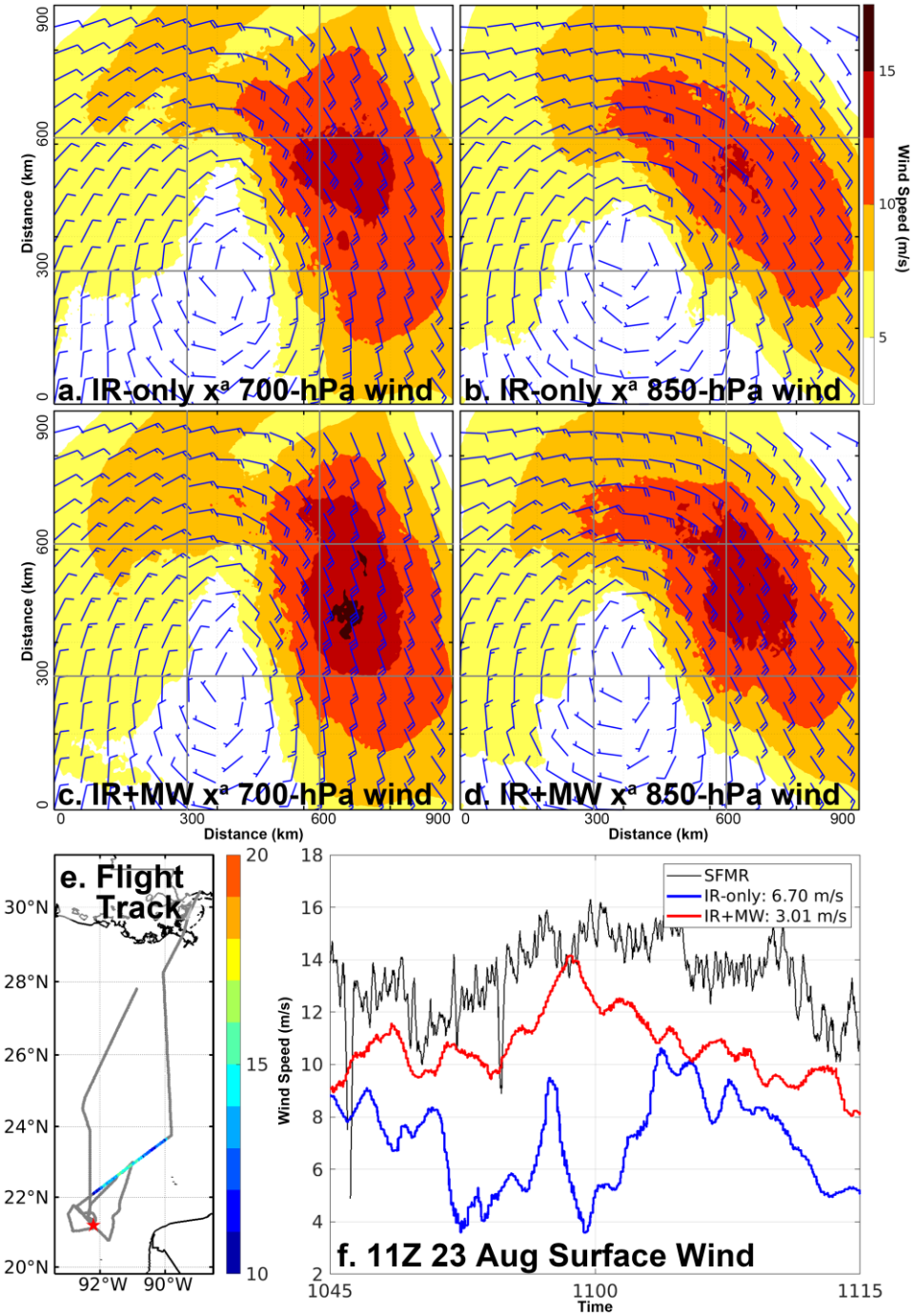

Figure 3. (a, c) 700-hPa and (b, d) 850-hPa horizontal winds (barbs) and wind speeds (shading) from the EnKF analyses of the (a, b) IR-only and (c, d) IR+MW experiment averaged every 6 hours from 1800 UTC 22 August through 1200 UTC 23 August. (e) Track of the reconnaissance flight (grey) with the colored section showing SFMR surface wind speeds from 1045 UTC to

1115 UTC 23 August; the red star marks Harvey's center using NHC best track data. (f) Comparisons of SFMR-retrieved wind speeds from 1045 UTC to 1115 UTC 23 August with those from the IR-only and IR+MW experiment EnKF analyses at 1100 UTC 23 August. (The numbers within the legend represent RMSEs between the SFMR-retrieved wind speeds and those from the EnKF analysis.)

The forecast errors for intensity, in terms of either minimum sea-level pressure or maximum surface wind speed, are also reduced when MW BTs are assimilated. There is a clear bifurcation in the IR-only forecasts (Figs. 2b,c): forecasts initialized before 0000 UTC 24 August are not able to capture the RI of Harvey, whereas the forecasts initialized after 0600 UTC 24 August do. The period from 0000 UTC to 0600 UTC 24 August is when the convection starts to become more organized (figure not shown), contributing to the RI of Harvey shortly thereafter. For the IR-only experiment, the lack of direct information on TC organization within the IR BTs may have hindered or delayed the RI of Harvey in the IR-only forecasts originating from times before 0000 UTC 24 August.

The addition of MW observations resulted in forecasts that captured the RI of Harvey, even those forecasts that are initialized within 24 hours of the start of the cycling EnKF (Figs. 2e,f). Furthermore, the assimilation of MW observations also resulted in forecasts with smaller mean absolute errors in intensity, with the largest error reductions around 40% at 60-h forecast lead times (Figs. 2h,i; statistically significant at 95% confidence level between 42 to 78 hours for minimum sea-level pressure and 48 to 60 hours for maximum surface wind speed). These forecast intensity improvements, especially in the early forecasts initialized before the observed RI of Harvey, likely result from changes in the TC's structures introduced by all-sky MW BT assimilation. The initial conditions for the first four forecasts from the IR+MW experiment have higher wind speeds associated with stronger cyclonic circulation in the lower troposphere (Figs. 3c,d) compared with those of the IR-only experiment (Figs. 3a,b). The higher wind speeds in the IR+MW experiment better match SFMR-retrieved surface wind speed (not assimilated) from a reconnaissance flight that covered the northeast quadrant of Harvey (Figs. 3e,f). A stronger cyclonic circulation in the IR+MW experiment likely enabled this experiment to produce more accurate forecasts of the onset of Harvey's RI than the IR-only experiment.

The assimilation of all-sky MW BTs also improves Harvey's rainfall forecasts. Figure 4 shows the accumulated rainfall forecasts from both experiments for the period from 0000 UTC 26 August through 0000 UTC 27 August, along with Stage-IV rainfall estimates (Lin and Mitchell 2005). The Stage-IV estimates reveal intense rainfall near Harvey's center as well as in the rainband to the northeast of the center (Fig. 4a). Both intense rainfall regions contributed to widespread flash flooding. To compare the performance of the two experiments, Equitable Threat Scores (ETS; Wilks 2011) were calculated for a range of verification rainfall thresholds and aggregated across all 10 forecasts. The ETS values (Fig. 4b) reveal that the IR+MW experiment forecasts have more accurate rainfall predictions than the IR-only experiment forecasts at all verification rainfall thresholds, ranging from almost +0.07 greater for the 5-mm threshold to more than +0.04 greater for the 100-mm threshold.

Differences between rainfall amount forecasts and Stage-IV estimates for the two experiments at two different times are also presented in Fig. 4. The 0000 UTC 23 August IR-only experiment forecasts are characterized by noticeable track forecast errors (Fig. 3a);

therefore, a dipole structure is visible in its differences with the Stage-IV estimates (Fig. 4c). With the track forecast errors reduced, the dipole structure disappears in the IR+MW experiment forecasts (Fig. 4e). Moreover, the severe underestimation of rainfall outside the core region in the southwest and northwest quadrants relative to the core in the IR-only experiment forecasts (Fig. 4c) is greatly reduced in the IR+MW experiment forecasts (Fig. 4e). This is likely the result of better analyses of the TC rainbands (e.g., Fig. 2), leading to an RMSE reduction from 63.96 mm to 48.77 mm. For the 0000 UTC 25 August forecasts for which both experiments have small track errors, the IR+MW experiment forecast still outperforms the IR-only experiment forecast with smaller biases, especially for the outer rainbands to the northeast over Houston. These smaller biases again led to more accurate rainfall amounts overall (Figs. 4d,f). These results show that assimilating all-sky MW BTs leads to substantial improvements in the accuracy of rainfall prediction during the landfall of TC Harvey.

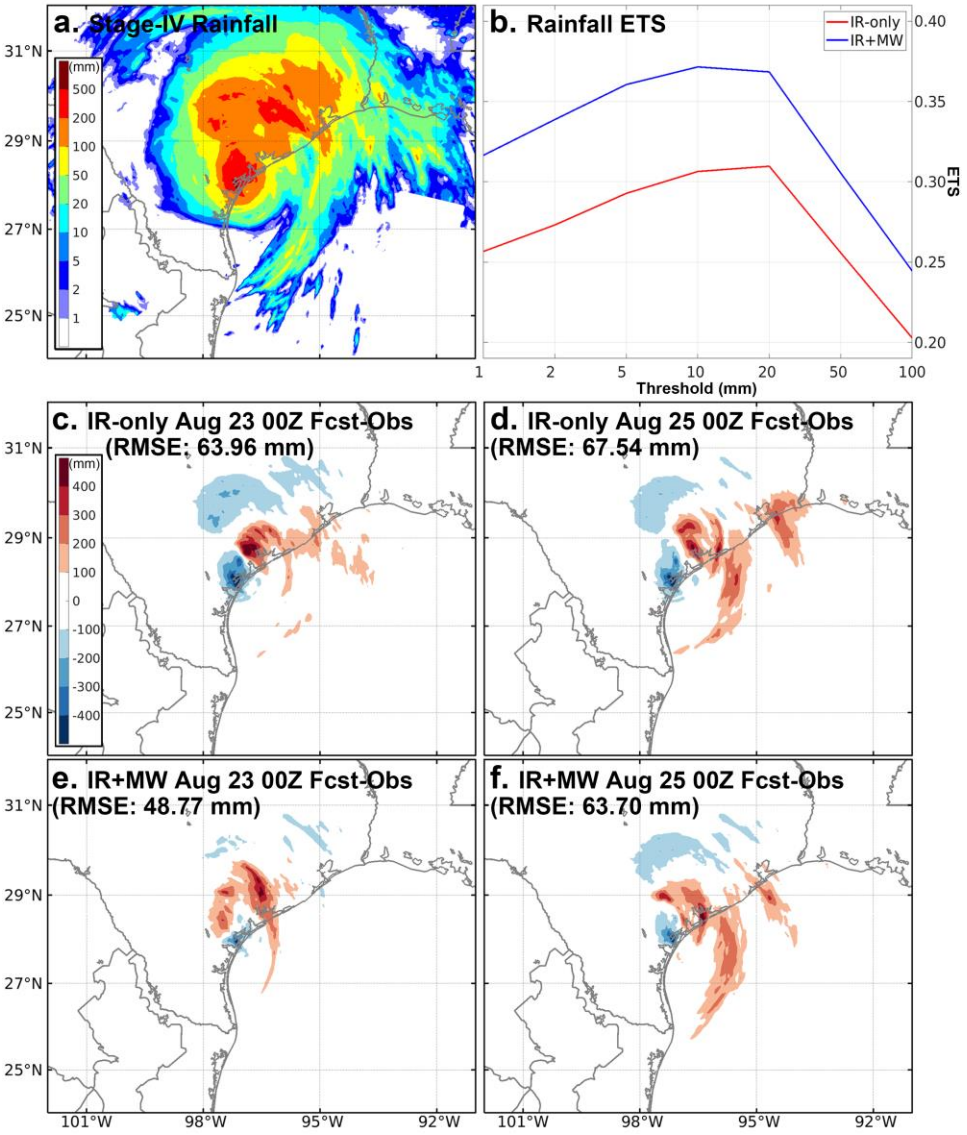

Figure 4. (a) Stage-IV total rainfall estimates accumulated from 0000 UTC 26 August through 0000 UTC 27 August. (b) Equitable Threat Scores (ETS) with different thresholds on rainfall amount from 0000 UTC 26 August through 0000 UTC 27 August for the predicted rainfall

averaged over all the forecasts. Forecast minus observed rainfall amount differences from the (c,) 0000 UTC 23 August and (d,f) 0000 UTC 25 August forecasts for the (c,d) IR-only and (e, f) IR+MW experiments for rainfall amounts accumulated from 0000 UTC 26 August through 0000 UTC 27 August.

4 Concluding remarks

This study reveals the value of assimilating all-sky MW BTs from low-Earth-orbiting satellites for improving the prediction of TC track, intensity, and precipitation through a case study of Hurricane Harvey (2017). This work builds upon recent successes in improving TC prediction through ensemble-based assimilation of all-sky IR BTs from geostationary satellites. Cloud-top information from the IR BTs in combination with information on the hydrometeors beneath the cloud tops from the MW BTs leads to better estimates of Harvey's structure. These improvements from assimilating all-sky MW BT lead to more accurate track and intensity forecasts and earlier accurate predictions of Harvey's RI, especially when the TC circulation was not yet well established. In addition, better representation of Harvey's structure following MW assimilation resulted in better rainfall forecasts after Harvey's landfall.

This is the first study to demonstrate improvements in track, intensity, and rainfall forecasts for a TC via assimilation of all-sky MW BTs in an ensemble-based convection-permitting data assimilation system. The influence of MW assimilation on TC prediction also depends upon AOEI, ABEI, and implementation of microphysics-consistent ice-particle scattering properties based on non-spherical ice particles.

Many challenges remain in the effective assimilation of all-sky MW BTs in support of predicting TCs and their associated hazards. Appropriate adaptive bias correction and localization for all-sky BT assimilation remain unresolved challenges. Comparisons of the low-frequency and high-frequency MW channel BTs from different analyses suggest that the performance of assimilating all-sky MW BTs using multiple channels depends on the choice of microphysics schemes, which will eventually impact the performance of the subsequent forecasts. Therefore, in order to better assimilate all-sky multi-channel MW BTs, there is a pressing need to develop microphysics schemes that more realistically simulate hydrometeors and/or observation operators that account for the uncertainties in microphysical processes. Nevertheless, our study demonstrates that, despite model, observation, and data assimilation deficiencies, there are benefits from the assimilation of the currently underutilized all-sky MW BTs for the prediction of TCs and their associated hazards.

Acknowledgments

When our dear friend and colleague Fuqing Zhang died unexpectedly in July 2019, the thread of ideas that wove together our ongoing combined infrared and microwave radiance data assimilation experiments unraveled. Members of the Center for Advanced Data Assimilation and Predictability Techniques, the center that Fuqing created here in the Department of Meteorology and Atmospheric Science at The Pennsylvania State University, came together over an extended period of time to reassemble the thread as best as possible. This paper is the result, and for most of us it will be the last one as a co-author with Fuqing.

This work is supported by NASA award 80NSSC19K0728, ONR award N000141812517, NOAA awards NA18OAR4590369 and NA18NWS4680054, NSF award AGS-1712290, and the Office of Science of DOE Biological and Environmental Research as part

of the Regional and Global Modeling and Analysis program area (project WACCEM). The numerical experiments were performed on the Stampede 2 supercomputer of the Texas Advanced Computing Center (TACC) through the Extreme Science and Engineering Discovery Environment (XSEDE) program supported by the National Science Foundation (NSF).

Data Availability

All observations and global model analyses and forecasts are downloadable from their publicly available archives. The EnKF analyses and deterministic forecasts produced by the IR-only and MW+IR experiments are available at http://hfip.psu.edu/yuz31/Zhangetal2021GRL/.

References

Blake, E. S., & Zelinsky, D. A. (2018). National Hurricane Center tropical cyclone report: Hurricane Harvey (AL092017). National Hurricane Center, 77 pp. https://www.nhc.noaa.gov/data/tcr/AL092017_Harvey.pdf.

Cangialosi, J. P., Blake, E., DeMaria, M., Penny, A., Latto, A., Rappaport, E., & Tallapragada, V. (2020). Recent progress in tropical cyclone intensity forecasting at the National Hurricane Center. *Weather and Forecasting*, *35*(5), 1913–1922.

Chan, M., Zhang, F., Chen, X., & Leung, L. R. (2020). Potential impacts of assimilating all-sky satellite infrared radiances on convection-permitting analysis and prediction of tropical convection. *Monthly Weather Review*, *148*(8), 3203–3224.

Chen, X., & Zhang, F. (2019). Development of a convection-permitting air-sea-coupled ensemble data assimilation system for tropical cyclone prediction. *Journal of Advances in Modeling Earth Systems*, *11*(11), 3474–3496.

Chow, K. C., Chan, K. L., & Lau, A. K. H. (2002). Generation of moving spiral bands in tropical cyclones. *Journal of the Atmospheric Sciences*, *59*(20), 2930–2950.

Christophersen, H. W., Dahl, B. A., Dunion, J. P, Rogers, R. F., Marks, F. D., Atlas, R., & Blackwell, W. J. (2021). Impact of TROPICS radiances on tropical cyclone prediction in an OSSE. *Monthly Weather Review*, *149*(7), 2279–2298.

Conrick, R., & Mass, C. F. (2019). Evaluating simulated microphysics during OLYMPEX using GPM satellite observations. *Journal of the Atmospheric Sciences*, *76*(4), 1093–1105.

DeMaria, M., Sampson, C. R., Knaff, J. A., & Musgrave, K. D. (2014). Is Tropical Cyclone intensity guidance improving? *Bulletin of the American Meteorological Society*, *95*(3), 387–398.

Diercks, J. W., & Anthes, R. A. (1976). Diagnostic studies of spiral rainbands in a nonlinear hurricane model. *Journal of Atmospheric Sciences*, *33*(6), 959–975.

Dudhia, J. (1996). A multi-layer soil temperature model for MM5. The 6th PSU/NCAR Mesoscale Model Users' Workshop, 3 pp.

Dvorak, V. F. (1975). Tropical cyclone intensity analysis and forecasting from satellite imagery. *Monthly Weather Review*, *103*(5), 420–430.

Galarneau, T. J., Jr., Bosart, L. F., & Schumacher, R. S. (2010). Predecessor rain events ahead of tropical cyclones. *Monthly Weather Review*, *138*(8), 3272–3297.

Geer, A. J., & Coauthors (2018). All-sky satellite data assimilation at operational weather forecasting centres. *Quarterly Journal of the Royal Meteorological Society*, *144*(713), 1191–1217.

Gustafson, N., & Coauthors (2018). Survey of data assimilation methods for convective-scale numerical weather prediction at operational centres. *Quarterly Journal of the Royal Meteorological Society*, *144*(713), 1218–1256.

Hartman, C., Chen, X., Clothiaux, E. E., & Chan, M.-Y. (2021). Improving the analysis and forecast of Hurricane Dorian (2019) with simultaneous assimilation of GOES-16 all-sky infrared brightness temperatures and tail Doppler radar radial velocities. *Monthly Weather Review*, *149*(7), 2193–2212.

Han, Y., Delst, P. v., Liu, Q., Weng, F., Yan, B., Treadon, R., & Derber, J. (2006). JCSDA Community Radiative Transfer Model (CRTM) – Version 1. NOAA Technical Report 122, 33 pp.

Honda, T., Miyoshi, T., Lien, G., Nishizawa, S., Yoshida, R., Adachi, S. A., Terasaki, K., Okamoto, K., Tomita, H., & Bessho, K. (2018). Assimilating all-sky Himawari-8 satellite infrared radiances: A case of Typhoon Soudelor (2015). *Monthly Weather Review*, *146*(1), 213–229.

Hong, S.-Y., & Lim, J.-O. J. (2006). The WRF single-moment 6-class microphysics scheme (WSM6). *Journal of the Korean Meteorological Society*, *42*(2), 129–151.

Hong, S., Noh, Y., & Dudhia, J. (2006). A new vertical diffusion package with an explicit treatment of entrainment processes. *Monthly Weather Review*, *134*(9), 2318–2341.

Hou, A. Y., Kakar, R. K., Neeck, S., Azarbarzin, A. A., Kummerow, C. D., Kojima, M., Oki, R., Nakamura, K., & Iguchi, T. (2014). The Global Precipitation Measurement Mission. *Bulletin of the American Meteorological Society*, *95*(5), 701–722.

Iacono, M. J., Delamere, J. S., Mlawer, E. J., Shephard, M. W., Clough, S. A., & Collins, W. D. (2008). Radiative forcing by long-lived greenhouse gases: Calculations with the AER radiative transfer models. *Journal of Geophysical Research: Atmospheres*, *113*(D13), D13103.

Jiménez, P. A., Dudhia, J., González-Rouco, J. F., Navarro, J., Montávez, J. P., & García-Bustamante, E. (2012). A revised scheme for the WRF surface layer formulation. *Monthly Weather Review*, *140*(3), 898–918.

Kidder, S. Q., Knaff, J. A., Kusselson, S. J., Turk, M., Ferraro, R. R., & Kuligowski, R. J. (2005). The Tropical Rainfall Potential (TRaP) technique. Part I: Description and examples. *Weather and Forecasting*, *20*(4), 456–464.

Kim, M.-J., Jin, J., Akkraoui, McCarty, W., Todling, R., Gu, W., & Gelaro, R. (2020). The framework for assimilating all-sky GPM Microwave Imager brightness temperature data in the NASA GEOS data assimilation system. *Monthly Weather Review*, *148*(6), 2433–2455.

Lin, Y., & Mitchell, K. E. (2005). The NCEP stage II/IV hourly precipitation analyses: Development and applications. Proceedings of the 19th Conference Hydrology, American Meteorological Society, San Diego, CA, USA (Vol. 10).

Meng, Z., & Zhang, Y. (2012). On the squall lines preceding landfalling tropical cyclones in China. *Monthly Weather Review*, *140*(2), 445–470.

Montgomery, M.T., & Kallenbach, R.J. (1997). A theory for vortex Rossby-waves and its application to spiral bands and intensity changes in hurricanes. *Quarterly Journal of the Royal Meteorological Society*, *123*(538), 435–465.

Minamide, M., & Zhang, F. (2017). Adaptive observation error inflation for assimilating all-sky satellite radiance. *Monthly Weather Review*, *145*(3), 1063–1081.

Minamide, M., & Zhang, F. (2018). Assimilation of all-sky infrared radiances from Himawari-8 and impacts of moisture and hydrometer initialization on convection-permitting tropical cyclone prediction. *Monthly Weather Review*, *146*(10), 3241–3258.

Minamide, M, & Zhang, F. (2019). An adaptive background error inflation method for assimilating all-sky radiances. *Quarterly Journal of the Royal Meteorological Society*, *145*(719), 805–823.

Minamide, M., Zhang, F., & Clothiaux, E. E. (2020). Nonlinear forecast error growth of rapidly intensifying Hurricane Harvey (2017) examined through convection-permitting ensemble assimilation of GOES-16 all-sky radiances. *Journal of the Atmospheric Sciences*, *77*(12), 4277–4296.

Rappaport, E. N. (2014). Fatalities in the United States from Atlantic tropical cyclones: New data and interpretation. *Bulletin of the American Meteorological Society*, *95*(3), 341–346.

Schmit, T. J., Griffith, P., Gunshor, M. M., Daniels, J. M., Goodman, S. J., & Lebair, W. J. (2017). A closer look at the ABI on the GOES-R series. *Bulletin of the American Meteorological Society*, *98*(4), 681–698.

Sieron, S. B., Clothiaux, E. E., Zhang, F., Lu, Y., & Otkin, J. A. (2017). Comparison of using distribution-specific versus effective radius methods for hydrometeor single-scattering properties for all-sky microwave satellite radiance simulations with different microphysics parameterization schemes. *Journal of Geophysical Research: Atmospheres*, *122*(13), 7027–7046.

Sieron, S. B., Zhang, F., Clothiaux, E. E., Zhang, L. N., & Lu, Y. (2018). Representing precipitation ice species with both spherical and nonspherical particles for radiative transfer modeling of microphysics-consistent cloud microwave scattering properties. *Journal of Advances in Modeling Earth Systems*, *10*(4), 1011–1028.

Sieron, S (2020). Passive microwave forward modeling and ensemble-based data assimilation within a regional-scale tropical cyclone model (Doctoral dissertation). University Park, PA: The Pennsylvania State University.

Skamarock, W. C., & Coauthors (2008). A description of the Advanced Research WRF version 3. NCAR Technical Note NCAR/TN-4751STR, 113pp.

Skofronick-Jackson, G., Petersen, W. A., Berg, W., Kidd, C., Stocker, E. F., Kirschbaum, D. B., Kakar, R., Braun, S. A., Huffman, G. J., Iguchi, T., Kirstetter, P. E., Kummerow, C., Meneghini, R., Oki, R., Olson, W. S., Takayabu, Y. N., Furukawa, K., & Wilheit, T. (2017). The Global Precipitation Measurement (GPM) mission for science and society. *Bulletin of the American Meteorological Society*, *98*(8), 1679–1695.

Thompson, G., Field, P. R., Rasmussen, R. M., & Hall, W. D. (2008). Explicit forecasts of winter precipitation using an improved bulk microphysics scheme. Part II: Implementation of a new snow parameterization. *Monthly Weather Review*, *136*(12), 5095–5115.

Tiedtke, M. (1989). A comprehensive mass flux scheme for cumulus parameterization in large-scale models. *Monthly Weather Review*, *117*(8), 1779–1800.

Velden, C., & Coauthors (2006). The Dvorak tropical cyclone intensity estimation technique: A satellite-based method that has endured for over 30 years. *Bulletin of the American Meteorological Society*, *87*(9), 1195–1210.

Wang, Y. (2002). Vortex Rossby waves in a numerically simulated tropical cyclone. Part II: The role in tropical cyclone structure and intensity changes. *Journal of the Atmospheric Sciences*, *59*(7), 1239–1262.

Weng, Y., & Zhang, F. (2012). Assimilating airborne Doppler radar observations with an ensemble Kalman filter for convection-permitting hurricane initialization and prediction: Katrina (2005). *Monthly Weather Review*, *140*(3), 841–859.

Weng, Y., & Zhang, F. (2016). Advances in convection-permitting tropical cyclone analysis and prediction through EnKF assimilation of reconnaissance aircraft observations. *Journal of the Meteorological Society of Japan*, *94*(4), 345–358.

Whitaker, J. S., & Hamill, T. M. (2002). Ensemble data assimilation without perturbed observations. *Monthly Weather Review*, *130*(7), 1913–1924.

Wilks, D. S. (2011). *Statistical methods in the atmospheric sciences*. Oxford, UK: Academic Press.

Wu, T., Zupanski, M., Grasso, L. D., Kummerow, C. D., & Boukabara, S. (2019). All-sky radiance assimilation of ATMS in HWRF: A demonstration study. *Monthly Weather Review*, *147*(1), 85–106.

Xu, D., Shen, F., Min, J., & Shu, A. (2021). Assimilation of GPM Microwave Imager radiance for track prediction of typhoon cases with the WRF Hybrid En3DVAR System. *Advances in Atmospheric Sciences*, *38*(6), 983−993.

Zhang, C., Wang, Y., & Hamilton, K. (2011). Improved representation of boundary layer clouds over the Southeast Pacific in ARW-WRF using a modified Tiedtke cumulus parameterization scheme. *Monthly Weather Review*, *139*(11), 3489–3513.

Zhang, F., & Weng, Y. (2015). Predicting hurricane intensity and associated hazards: A five-year real-time forecast experiment with assimilation of airborne Doppler radar observations. *Bulletin of the American Meteorological Society*, *96*(1), 25–33.

Zhang, F., Minamide, M., & Clothiaux, E. E. (2016). Potential impacts of assimilating all-sky infrared satellite radiances from GOES-R on convection-permitting analysis and prediction of tropical cyclones. *Geophysical Research Letters*, *43*(6), 2954–2963.

Zhang, F., Snyder, C., & Sun, J. (2004). Impacts of initial estimate and observation availability on convective-scale data assimilation with an ensemble Kalman filter. *Monthly Weather Review*, *132*(5), 1238–1253.

Zhang, F., Weng, Y., Gamache, J. F., & Marks, F. D. (2011). Performance of convection-permitting hurricane initialization and prediction during 2008–2010 with ensemble data assimilation of inner-core airborne Doppler radar observations. *Geophysical Research Letters*, *38*(15), L15810.

Zhang, F., Weng, Y., Sippel, J. A., Meng, Z., & Bishop, C. H. (2009). Cloud-resolving hurricane initialization and prediction through assimilation of Doppler radar observations with an ensemble Kalman filter. *Monthly Weather Review*, *137*(7), 2105–2125.

Zhang, F., Minamide, M., Nystrom, R. G., Chen, X., Lin, S., & Harris, L. M. (2019). Improving Harvey forecasts with next-generation weather satellites: Advanced hurricane analysis and prediction with assimilation of GOES-R all-sky radiances. *Bulletin of the American Meteorological Society*, *100*(7), 1217–1222.

Zhang, Y., Stensrud, D. J., & Clothiaux, E. E. (2021a). Benefits of the Advanced Baseline Imager (ABI) for ensemble-based analysis and prediction of severe thunderstorms, *Monthly Weather Review*, *149*(2), 313–332.

Zhang, Y., Clothiaux, E. E., & Stensrud, D. J. (2021b). Correlation structures between satellite all-sky infrared brightness temperatures and the atmospheric state at storm scales. *Advances in Atmospheric Sciences*, in press, doi:10.1007/s00376-021-0352-3.

Zhang, Y., Chen, X., & Lu, Y. (2021c). Structure and dynamics of ensemble correlations for satellite all-sky observations in an FV3-based global-to-regional nested convection-permitting ensemble forecast of Hurricane Harvey. *Monthly Weather Review*, *149*(7), 2409–2430.

512 **Appendix**

513 **Appendix A.** List of acronyms

514 ABEI – Adaptive Background Error Inflation
515 ABI – Advanced Baseline Imager
516 AMSR2 – Advanced Microwave Scanning Radiometer 2
517 AOEI – Adaptive Observation Error Inflation
518 ARW – Advanced Research WRF model
519 ATMS – Advanced Technology Microwave Sounder
520 BT – Brightness temperature
521 CRTM – Community Radiative Transfer Model
522 DMSP – Defense Meteorological Satellite Program
523 EnKF – Ensemble Kalman filter
524 ETS – Equitable Threat Score
525 GCOM-W1 – Global Change Observation Mission 1st - Water
526 GMI – GPM Microwave Imager
527 GPM – Global Precipitation Measurement project
528 GOES – Geostationary Operational Environmental Satellite
529 IR – Infrared
530 MHS – Microwave Humidity Sounder
531 MW – Microwave
532 NHC – National Hurricane Center
533 NOAA – National Oceanic and Atmospheric Administration
534 PBL – Planetary boundary layer
535 PSU – The Pennsylvania State University
536 RI – Rapid intensification
537 RMSE – Root-mean-square error
538 RRTMG – Rapid Radiative Transfer Model for Global Circulation Model
539 TC – Tropical cyclone
540 SAPHIR – Sounder for Probing Vertical Profiles of Humidity
541 SFMR – Stepped-Frequency Microwave Radiometer
542 SSM/I – Special Sensor Microwave/Imager
543 SSMIS – Special Sensor Microwave Imager/Sounder
544 Suomi NPP – Suomi National Polar-orbiting Partnership

545 WPC – Weather Prediction Center
546 WRF – Weather Research and Forecasting model
547 WRFDA – WRF Data Assimilation system
548 YSU – Yonsei University

549 **Appendix B.** Assimilated channels from the GPM constellation sensors.

Sensor	**Satellite**	**LF Channel**	**HF Channel**
AMSR2	GCOM-W1	7 (18.7 GHz)	13 (89.0 GHz)
ATMS	Suomi NPP		18 (183.31±7.0 GHz)
GMI	GPM Core Observatory	3 (18.7 GHz)	13 (183.31±7.0 GHz)
MHS	NOAA-18		5 (190.31 GHz)
SAPHIR	Megha-Tropiques		5 (183.31±6.6 GHz)
SSM/I	DMSP-F15	1 (19.35 GHz)	6 (85 GHz)
SSMIS	DMSP-F16, F17, F18	13 (19.35 GHz)	9 (183.31±6.6 GHz)

550